



Published in final edited form as:

Mol Imaging. 2011 August ; 10(4): 305–316. doi:10.2310/7290.2010.00054.

Rh-I-UEA-1 polymerized liposomes target and image adenomatous polyps in the APC^{Min/+} mouse using optical colonography

Celeste A. Roney^{1,a}, Biying Xu^{1,b}, Jianwu Xie^{1,a}, Shuai Yuan², Jeremiah Wierwille², Chao-Wei Chen², Yu Chen², Gary L. Griffiths^{1,b}, and Ronald M. Summers^{1,a,*}

¹National Institutes of Health, Bethesda, MD, 20892, USA

^aImaging Biomarkers and Computer-Aided Diagnosis Laboratory, Radiology and Imaging Sciences Department, Clinical Center, Bldg 10, Room 1C368X, MSC 1182

^bThe Imaging Probe Development Center, National Heart, Lung, and Blood Institute, 9800 Medical Center Drive, Bldg B, Bldg 10, Room 9D06

²Fischell Department of Bioengineering, University of Maryland, College Park, MD, 20742, USA

Abstract

Mutated adenomatous polyposis coli (APC) genes predispose transformations to neoplasia progressing to colorectal carcinoma (CRC). Early detection facilitates clinical management and therapy. Novel lectin-mediated polymerized targeted liposomes (Rh-I-UEA-1), with polyp specificity and incorporated imaging agents, were fabricated to locate and image adenomatous polyps in APC^{Min/+} mice. The biomarker α -L-fucose covalently joins liposomal conjugated lectin *ulex europaeus* agglutinin (UEA-1), via glycosidic linkage to the polyp mucin layer. Multispectral optical imaging (MSI) corroborated a global perspective of specific binding (Rhodamine B 532 nm emission, 590–620 nm excitation) of targeted Rh-I-UEA-1 polymerized liposomes to polyps with 1.4 \times fold labeling efficiency. High-resolution co-registered optical coherence tomography (OCT) and fluorescence molecular imaging (FMI) reveal spatial correlation of contrast distribution and tissue morphology. Freshly excised APC^{Min} bowels were incubated with targeted liposomes (UEA-1 lectin), control liposomes (no lectin), or Omnipaque and imaged by the three techniques. CT quantitative analyses did not confirm targeted liposomes more strongly bound polyps than nontargeted liposomes or Omnipaque alone. OCT, with anatomical depth capabilities, along with the co-registered FMI, substantiated Rh-I-UEA-1 liposome binding along the mucinous polyp surface. UEA-1 lectin denotes α -L-fucose biomarker carbohydrate expression at the mucin glycoprotein layer; Rh-I-UEA-1 polymerized liposomes target and image adenomatous polyps in APC^{Min} mice.

Keywords

colorectal carcinoma; adenomatous polyps; *ulex europaeus* agglutinin; polymerized liposome; small animal imaging

1. Introduction

The pathology of colorectal carcinoma (CRC) evolves through normal colon, adenoma, adenoma with high grade dysplasia, and invasive adenocarcinoma ¹. Biomarkers of CRC

*To whom correspondence should be addressed. rms@nih.gov.

may spawn from colonocytes, and these biomarkers may be detectable either in feces or by targeted molecular imaging. Lectins are plant and animal proteins having specific sugar moiety affinities, and a range of functions, from cell-cell recognition and adhesion, to glycoprotein synthesis. Lectin-binding sites and regional binding differences have been observed in association with colorectal lesions. Clinical specimens of normal mucosa and cancerous lesions were examined with the lectin *Ulex europaeus* agglutinin-1 (UEA-1).² The authors² found 82 % binding of UEA-1 by carcinomas of the rectum, whereas 0 % binding was observed in the normal mucosa of the rectum; UEA-1 binding differences between the right and left colon were also reported. Primarily, in the left colon, cancerous tissue bound UEA-1 79 % versus 10 % UEA-1 binding of nonneoplastic mucosa; UEA-1 binding in the right colon was reported as 71 % for carcinoma, with 100 % UEA-1 binding for the normal mucosa. A correlation was suggested between positive UEA-1 binding in rectal carcinoma and the α -L-fucose glycoprotein.²

In an animal study of lectin-binding sites³, rat mucosa artificially induced with the carcinogen 1,2-dimethylhydrazine (DMH) to undergo colonic transformation, positively bound the lectins UEA-1 and PNA, versus non-DMH treated rats. The authors report 100 % distal and proximal colon carcinoma labeling with UEA-1, and 50 % and 60 % carcinoma labeling in the proximal and distal colon, respectively, with PNA. In the same study³, a labeling discrepancy was reported between regions of the colon in the non-DMH treated rats with UEA-1. For example, the lectin labeled 100 % of the proximal tissue, and 0 % of the distal colon; these findings resemble similar clinical results². The PNA lectin labeled neither the distal nor the proximal colon in the control rats.

UEA-1 modified polymerized liposome for targeting M cell as an oral vaccine vehicle was originally reported by Chen et al⁴ using polymerizable lipid, DODPC. In recent years, a UV polymerizable diacetylenic phosphatidylcholine 1,2-bis(tricosano-10,12-diyne)-sn-glycero-3-phosphocholine (DAPC) was found to form stable liposome with DMPC in buffer and plasma⁵, a 1:1 ratio of DAPC to DMPC polymerized efficiently with a relatively high stability⁶. To exploit the affinity of lectins for the mucin carbohydrate backbone, we have conjugated UEA-1 onto the outer surfaces of polymerized liposomes, which have Rhodamine, and are also encapsulated with an iodine imaging contrast agent, Omnipaque. UEA-1 was selected as a ligand of interest because polyps may secrete surface mucins. The murine model of CRC, *APC^{Min/+}*, was used to show that Rh-I-UEA-1 liposomes are targeted to polyps, surface bound and detectable by the imaging modalities MSI, μ CT, and OCT + FMI.

2. Methods

2.1. Lectin Immunohistochemistry

Paraffinized intestinal sections containing adenomatous polyps (N=13 specimen) were obtained from heterozygous male C57BL/6J *APC^{Min/+}* mice (The Jackson Laboratories, Bar Harbor, ME, stock 002020, 8 wks, 25 g.). The paraffin was warmed by heating the tissue sections to 60° C for 30 mins; warmed paraffin sections were deparaffinized in 3X xylene, 100 % ethanol (EtOH), 75 % EtOH, 50 % EtOH, and H₂O. The final wash was in PBS. The sections were incubated in two antibody blocking solutions for 10 mins and 30 mins, respectively. Lectin staining for carbohydrate expression was performed overnight at 4 ° C. Fluorescein (FITC)-labeled lectins were commercially purchased (in a kit) from Vector Laboratories (Burlingame, CA, USA). The lectins were diluted 1:500, using antibody diluent (Zymed[®], Carlsbad, CA), to a final concentration of 5 μ g/mL; the FITC-lectins used in this experiment were: Concanavalin A (ConA), Dolichos biflorus agglutinin (DBA), Peanut agglutinin (PNA), Ricinus communis agglutinin (RCA), Soybean agglutinin (SBA), *Ulex europaeus* agglutinin (UEA), Wheat germ agglutinin (WGA), Jacalin (Jac), and Sambucus

nigra agglutinin (SNA). The tissue sections were counterstained with DAPI, (2-(4-amidinophenyl)-1H-indole-6-carboxamide), and were subsequently viewed for carbohydrate expression by fluorescent microscopy.

2.2. Ex Vivo Multispectral Optical Imaging (MSI)

C57BL/6J APC^{Min/+} specimens were incubated in 200 μ L Rh-I-UEA-1 targeted polymerized liposomes or Rh-I-polymerized control liposomes for 30 minutes at room temperature in a closed Petri dish. The tissues were washed twice each in 1X PBS for 5 mins with shaking before MSI. For UEA-1 conjugated liposome studies, 27 polyps and 6 normal adjacent specimens were analyzed. Of the fresh specimens incubated with nonconjugated liposomes, 13 were studied as experimental polyps and 6 specimens were collected from mucosa of normal adjacent tissue. Multispectral optical imaging (MSI) was performed using a high sensitivity CRi MaestroTM imaging system (Woburn, MA). Imaging was performed at 10 nm intervals over the spectrum 500 nm to 720 nm, with an 800 msec exposure at each interval; the major peak was found at 560 nm. Background scatter was subtracted from the final reconstructed image. Representative bright field images were also photographed.

2.3. Polymerization of I-Rh-UEA-1 Conjugated Liposomes

Liposomes were made by the extrusion method. The total lipid in chloroform was dried to form a thin lipid film, which was hydrated with iodinated contrast solution, extruded and crosslinked to form polymerized liposomes. The UEA-1 was subsequently conjugated to the liposomes. Briefly, 40 μ mol of the polymerizable diacetylene phospholipid DAPC (1,2-bis(10,12-tricosadiynoyl)-*sn*-glycero-3-phosphocholine) (Avanti Polar Lipids, Alabaster, AL), was mixed with 40 μ mol of the saturated “spacer” lipid dimyristoylphosphatidylcholine DMPC (Lipoid, Newark, NJ), or functionalized lipid, DMPE-GLU (N-Glutaryl-L- α -phosphatidylethanolamine dimyristoyl) (NOF, Japan) with a 1:1 ratio together with 1 % (0.8 μ mol) of 18:1 Lissamine Rhodamine B PE (1,2-dioleoyl-*sn*-glycero-3-phosphoethanolamine-N-lissamine rhodamine B sulfonyl ammonium salt) (excitation 550 nm, emission 590 nm; Avanti Polar Lipids). The lipids in chloroform were added to a round bottom flask in the dark and protected with aluminum foil. Solvent was removed under reduced pressure and the phospholipids were dried further under high vacuum for 48 hours. The lipid film was hydrated in 1 mL EtOH and 9 mL (350 mg/mL) iodinated contrast solution (OmnipaqueTM, iohexol) from GE healthcare (Piscataway, NJ) for 2 hrs at 70 °C. The liposomes were extruded using a 10 mL LipexTM Thermobarrel Extruder (Northern Lipids Inc, Burnaby, BC, Canada), and polycarbonate filters with pore size of 100 nm. Extrusion was performed for 10 cycles in a water bath at 70 °C. The extruded liposomes were polymerized on ice using a Strategene Stratalinker[®] 1800 UV Crosslinker (La Jolla, CA). Cross-linking was performed at 3600 μ J per cycle for 20 cycles ⁶.

For UEA-1 conjugation, polymerized liposomes were exchanged into 0.1 M MES buffer (pH = 4.7) using a PD-10 column according to the manufacturer’s instructions. EDC (30 mg, 156 μ mol) and sulfo-NHS (85 mg, 383 μ mol) were added to the liposome solution and mixed for 10 minutes at room temperature. The liposomes were then exchanged into phosphate buffered saline (PBS, pH = 7.4) using a PD-10 column and 20 mg of UEA-1 in PBS buffer was added. The final concentration of UEA-1 in the reaction mixture was 1 mg/ml. The mixture was incubated at 4°C on a shaker, overnight. The mixture was then loaded onto a 100K Amicon ultrafiltration spin-column (Millipore) and washed with PBS (3 \times 10 mL) three times at 1000 g. This process was monitored by Agilent HPLC, TSK-G6000PW column was used with a flow rate of 1ml/min. More PBS wash was done until there was no unbound UEA-1. The flow-through of each centrifugation was collected and tested for UEA-1 amounts using a commercial BCA kit from Pierce (Rockford, IL). The amount of UEA-1 conjugated to polymerized liposomes was determined by subtracting the unbound

UEA-1 from the initial addition of 20 mg. Both control liposome and UEA-1 conjugated polymerized liposomes were analyzed by dynamic light scattering (DLS) using a Malvern Zetasizer ZS (Nanocomposix) and transmission electron microscopy (TEM). The liposomes were stored at 4 °C until further use.

2.4. Liposome Incubation of Formalin Fixed and Fresh Frozen Tissue

Freshly excised C57BL/6J APC^{Min/+} small and large bowels (N = 3) were quickly preserved in 4% paraformaldehyde and stored at -80 °C until further use. Additionally, male C57BL/6J APC^{Min/+} mouse bowels commercially purchased from the Jackson laboratories (Bar Harbor, ME) were used (N = 10). The bowels were incubated in 200 µL I-Rh-UEA-1 (targeted) liposome or control liposome (no UEA-1) for 30 minutes at room temperature in a closed Petri dish. The tissues were washed twice each in 1X PBS for 5 mins with shaking, before all imaging experiments.

2.5. Micro Computed Tomography Imaging

All fresh tissue described henceforth were incubated according to the experimental procedures outlined in section 2.2. For UEA-1 conjugated liposome studies, 27 polyps and 6 normal adjacent specimens were collected from male C57BL/6J APC^{Min/+} mice (Jackson Labs, ME). Upon tissue incubation and washing, and prior to imaging, the specimens were bonded to laminate bases (4 cm × 2 cm) with adhesive Super Glue[®]. Representative baseline µCT images were taken of corresponding experimental polyps and normal specimens; therefore, 27 baseline polyps were under review for the UEA-1 conjugated liposome study. Of the fresh specimens incubated with nonconjugated liposomes, 13 were studied as experimental polyps and 6 specimens were collected from mucosa of normal adjacent tissue. As described earlier, baseline µCT images were taken of corresponding experimental polyps and normal specimens; therefore, 13 baseline polyps were reviewed for the nonconjugated liposome study.

Micro CT imaging was achieved using a SkyScan 1172TM (Micro Photonics, Allentown, PA) high resolution µCT scanner. Imaging parameters were 80 kV with a frame average of 8, 125 µA, 0.5° rotation step, 35 µm pixel size, and 158 ms exposure. 3D reconstruction was executed with corrections for ring artifacts and beam hardening via the image reconstruction software NRecon (Skyscan[®], Kontich, Belgium). Image analyses were accomplished via the software program Data Viewer (version 1.3.2, Skyscan[®], Kontich, Belgium), and the public domain Java-based image processing program ImageJ. Data Viewer was implemented to manually determine the positions of the polyps in the X, Y and Z axes. Z axis slice numbers equivalent to the surfaces of the polyps were used as input for ImageJ voxel based region-of-interest (ROI) measurements at the polyp surface. The unit output of the ImageJ measurements was the grayscale. The grayscale values were converted to Hounsfield units (HU) based on experimental parameters and CT settings (i.e. normalization of water, kV, frame averaging). Five slices were measured, at the polyp surface, per polyp.

2.6. Optical Coherence Tomography (OCT) with Fluorescence Molecular Imaging (FMI)

Fresh tissue samples were incubated in Rh-I liposomes conjugated with and without the UEA-1 lectin as described throughout. N=4 tissue samples were used for OCT + FMI imaging.

Light is produced from wavelength-swept light by a high speed, high-resolution OCT operating system. It generates a broadband spectrum of 100 nm at 1300 nm, which provides an axial resolution of 10 µm in the tissue. The laser operates at a sweep rate of 16 kHz (equivalent to an imaging speed of 15 frames per second for a 1024 axial-line image) with an average output power of 12 mW. The system sensitivity is 95 dB. A Michelson

interferometer composed of one circulator and a fiberoptic 50/50 splitter is used to generate the Fourier-domain OCT signal. The OCT interference signal returned from both the sample and reference arms is detected by a balanced photodetector. A Mach-Zehnder interferometer (MZI) with a fixed path difference is used to create an optical frequency clock. Data acquisition is triggered by the zero-crossings of the MZI fringes, which are evenly spaced in optical frequency. Discrete Fourier transform (DFT) is performed on the data to generate an axial depth profile of the sample (A-line) with 3 mm imaging depth and 512 pixels ⁷.

The fluorescence molecular imaging (FMI) system uses a continuous-wave (CW) solid-state laser at 532 nm as the excitation source. The excitation light is combined with the OCT sample arm using a dichroic mirror. The typical illumination power on the sample is approximately 5 mW. The reflectance and fluorescence light is detected by the same fiber and then connected to a fiber splitter to divide the collected light into reflectance and fluorescence signals. The simultaneous measurement of reflectance and fluorescence signals from the same source and detector geometry is important for minimizing the influence of optical coupling variation for both excitation and collection paths. The reflectance signals are detected by avalanche photodiodes (APD), while the fluorescence signals first pass through an emission filter set (600 ± 10 nm), and then are detected by a photomultiplier tube (PMT). The illumination and filter wavelengths are chosen based on the excitation and emission properties of the fluorescent dye Rhodamine ⁸.

2.7. Statistical Analysis

Data were entered into Excel worksheets (Microsoft™ Corporation, Redmond, WA, USA) and analyzed using the non-paired, two-tailed Student's t test with unequal variance. $P < 0.05$ was regarded as significant. Statistical analyses were generated using the statistical software Minitab® (Minitab, Inc., State College, PA, USA) and MATLAB (The MathWorks Inc.™, Natick, MA, USA).

3. Results

3.1. Lectin Immunohistochemistry

Paraffin-fixed intestinal tissue sections (N=13 total; 9 initially, 4 repeated with best lectin) from male C57BL/6J APC^{Min/+} mice were deparaffinized and stained with 9 FITC-lectins each for immunohistochemistry analysis. 1/9 lectin, the FITC-UEA-1, stained the polyps but not the adjacent normal tissue (Figure 1). 3/9 lectins stained the normal mucosa, but not the polyp (RCA, ConA, PNA); 3/9 lectins stained the polyp with no differentiation over the normal mucosa (SNA, JAC, SBA); and 2/9 lectins showed carbohydrate expression at the polyp, *and* a high background in the normal tissue (WGA, DBA).

The image analysis and processing software ImageJ was used to measure average thickness along the mucin layer. As illustrated in Figure 1, the average thickness of the mucin layer was 53.44 ± 27.03 μm (N=20). When FITC-UEA-1 was used to incubate the colon tissue prior to slicing, fluorescence of the lectin label was indicated at the polyp surface, thereby confirming α -L-fucose carbohydrate expression, and suggesting UEA-1 as a viable ligand for surface targeting of polyps (Figure 2).

3.2. In Vitro Multispectral Optical Imaging

Twenty seven polyps and 6 normal adjacent tissues were studied for UEA-1 conjugated liposome incubation; 13 polyps and 6 normal adjacent tissues were investigated for nonconjugated liposome incubation. MSI showed positive correlation with specific binding of Rh-I-UEA-1 by the polyp. Within tissue comparisons of fluorescence intensity of Rh-I-UEA-1 labeled specimens yielded a target-to-background ratio of 1.74 (N=27; $240.91 \pm$

12.12; normal adjacent (N=6; 138.38 ± 11.46)). Similar evaluations of the control liposomes yielded a target-to-background fluorescence intensity ratio at the polyp of 1.34 (N=27; 171.49 ± 33.26 ; normal adjacent (N=6; 128.26 ± 31.89)). Accordingly, the polyp labeling efficiency of Rh-I-UEA-1 was significantly better ($P < 0.05$) by 1.4X, than that of the control liposomes (N=27; 240.91 ± 12.12 versus (N=6; 171.49 ± 33.26)). The polyps are distinctly identified when APC^{Min/+} tissues are incubated with Rh-I-UEA-1, whereas control liposomes (no UEA-1) do not label polyps (Figure 3). Figure 4 shows APC^{Min/+} tissue that has been incubated with Rh-I-UEA-1; the polyp is clearly labeled, and the normal mucosa has low nonspecific binding.

3.3. Polymerization of I-Rh-UEA-1 Conjugated Liposomes

A pictorial representation of the liposomes was shown in Figure 5a. The size distributions of both control and UEA-1 conjugated liposomes were analysed by DLS, the control liposomes were with a hydrodynamic size of 58.3 ± 11.29 nm (n=5) and UEA-1 conjugated liposomes with a size of 72.17 ± 8.95 nm (n=7). The size distributions of UEA-1 conjugated liposomes were stable over a period of two weeks in PBS. Figure 5b shows representative DLS of control and UEA-1 conjugated liposomes and Figure 5c TEM image of liposomes.

For determining the total amount of UEA-1 conjugated to the liposomes, flow from 100K Amicon Ultrafiltration columns was collected and quantified using BSA as standards. HPLC was used to monitor the purification process and sample analyses. UV absorbance at 550nm, rhodamine's UV absorbance wavelength, was used for monitoring liposomes, while UV absorbance at 280nm was used for detection of UEA-1. Figure 5d shows the HPLC of purified UEA-1 liposomes (retention time 8.4min). The total amount of UEA-1 conjugated to the liposomes was 4.11 ± 1.60 mg (n=7).

3.4 Micro Computed Tomography Imaging

Rh-I-UEA-1 liposomes qualitatively suggest targeted labeling of the polyps along the mucin surface, as shown in However, quantitative analyses of mean Hounsfield Units (HU, mean \pm SD), did not show preferential binding of the Rh-I-UEA-1 targeted liposomes at the polyp surface versus the nontargeted liposomes, due to beam hardening along the image periphery. Therefore, the results were inconclusive, and did not yield significance.

3.5. Optical Coherence Tomography with Fluorescence Molecular Imaging

Twenty eight total polyps were analyzed by OCT + FMI imaging (12 conjugated; 16 nonconjugated). The polyp-to-background ratio was significantly higher ($P < 10^{-6}$) in conjugated (1.45 ± 0.18) samples versus nonconjugated samples (0.74 ± 0.16) as shown in 9 shows the OCT + FMI compilations of an APC^{Min/+} specimen incubated with Rh-I-UEA-1. In the FMI profile, the targeted liposomes labeled the outer ring, or surface, of the polyps, identified as P in the image. There was residual background noise around the edges of the tissue due to liposomes sticking between the tissue and the laminate base, and incompletely washing away. The OCT height profile details the height of the polyp in relation to normal adjacent tissue, and the OCT cross section recognizes the distinguishing crypts of adenomatous polyps. Polyp height was 1 mm to 2.5 mm.

Contrary to the surface labeling found at the outer ring of the polyps by Rh-I-UEA-1, the nonconjugated liposomes did not label polyps. The OCT height profile and cross section of an APC^{Min/+} specimen incubated with nonconjugated liposomes correctly identified the polyp positions and characteristic crypts; however, from the FMI profile, there was no labeling of the polyps by nonconjugated liposomes. Again, background noise was inherent at the edges of the tissue.

4. Discussion

Polymerized liposomes have been suggested as oral vaccination vehicle with different lipid compositions⁴⁻⁶. DAPC and DMPC lipid composition was selected for this study due to the availability of both lipids and also this lipid composition has been studied extensively. Enhanced polymerization was reported when DMPC was added to DAPC with 1:1 ratio⁹ and liposomes with this composition exhibit relative stability in saliva when compared with other composition⁵; therefore this composition holds promise for oral delivery. In this study, novel lectin-mediated polymerized targeted liposomes, Rh-I-UEA-1, were fabricated to detect and image polyps in the APC^{Min/+} murine model of colon cancer. The lectin UEA-1, sensitive to the expression of the carbohydrate α -L-fucose, was selected as a labeling agent because the surface layer of the polyps may have a glycoprotein coating containing a mucin backbone. When conjugated onto liposomal vehicles with optical (Rhodamine) imaging agents, Rh-I-UEA-1 selectively bound to the polyp surface versus nonconjugated liposomes. Imaging was validated by MSI and OCT + FMI. Thus, Rh-I-UEA-1 is a promising candidate as a multimodality bioimaging label for polyp detection in CRC research.

The stimulus to produce a polyp specific contrast agent in the APC^{Min/+} model extrapolated from clinical findings in our laboratory, detailing the first quantitative CT colonography (CTC) results¹⁰ of oral contrast adherence to the surfaces of polyps. O'Connor *et al.*¹⁰ found 46 % surface tagging of polyps by oral contrast administration of barium sulfate (Ba₂SO₄) and Gastrografin. Increased attenuation of fecal matter distinguishes stool from polyps immersed in pools of oral contrast. Oral contrast homogeneously mixes with stool, appearing inside the stool on CT. However, with polyps, the contrast appears outside the object on CT because it coats the surfaces of the polyps. Radiologists must maintain prudence to avoid identification of false lesions¹¹, but nevertheless, it was a significant finding that 46 % of the polyps had a surface labeling of adherent contrast. Of especial clinical note, too, was that polyps with a villous component, associated with a greater risk of malignancy¹², had 77 % adherent contrast. Thus, outlines the motivation to design a marker with enhanced polyp specificity. In context with the hypothesis¹⁰ that atypical mucus production may underlie preferential oral contrast adherence to villous polyps, such a marker was sought, with the novel fabrication of Rh-I-UEA-1.

Mucins are high molecular weight glycoproteins located in the goblet cells that proliferate the crypts of the colon and rectum. Functions of the colonic intestinal mucin layer include nourishing the bacteria as a food source¹³, absorption of Na⁺¹⁴, and facilitating the binding of Ca²⁺ by intestinal goblet cells¹⁵. Mucin-associated carbohydrate expression becomes altered during the progression to malignancy in CRC¹⁶. MUC1 was implicated in reducing E-cadherin-assisted epithelial cell-cell adhesion when transfected into murine fibroblast cells (that do not independently demonstrate cell-cell communication) with E-cadherin cDNA¹⁷. Given MUC1s apparent role in inhibiting cellular adhesion, it was postulated that non-cohesion results from loss of cellular polarity; meanwhile, abnormal glycosylation may permit attachment of malignant cells to epithelia along the path to metastasis¹⁸. Nakamori *et al.*¹⁹ correlate MUC1 expression to the clinical stage of disease using surgically resected specimens of adenocarcinoma of the colon and rectum. The authors used two monoclonal antibodies, specific for heavily glycosylated MUC1, and underglycosylated MUC1, to demonstrate mature MUC1 expression in advanced disease¹⁹. In addition, it has been validated (using selective binding lectins to mucin in the human colon), that “alteration[s] in the exposed, nonreducing carbohydrate residues occurs in human colonic mucin during the process of goblet cell differentiation, and exposed carbohydrate structure[s] not normally present in human tissues [are] expressed in the mucin produced by malignant colonic epithelium”²⁰.

Gastrointestinal mucosal imaging has been reviewed in the literature²¹⁻²². Sodir *et al*²³ imaged an in-house mouse model of CRC, called *APC^{MIN/+}Smad3^{-/-}*, by small animal CT. This model is suggested to mimic familial adenomatous polyposis (FAP) because of solid polyp growth in the distal colon; however, crossing the two genes accelerates tumor growth, which is in contrast to the slow tumor growth represented by the human situation. The authors²³ demonstrated mutant colons with manifold polyps, but, the heavy metal barium was elected as the contrast medium. Barium, although common, is not a very selective imaging contrast agent. Therefore, the multiplicity of polyps generated by crossing *APC^{Min/+}* and *Smad3^{-/-}* were not faithfully represented by the *in vivo* images.

APC^{Min/+} specimens have also been analyzed by other imaging techniques, including OCT, laser-induced fluorescence (LIF)²⁴⁻²⁵, and laser-scanning confocal microscopy (LSCM)²⁵. The LIF technique exploits the autofluorescence of diseased or non-diseased tissue through excitation of endogenous fluorophores in a sample preparation of an exogenous dye. A spectral fingerprint is gained by shining ultraviolet light on the sample dye and collecting the tissue emission. LSCM combines LIF with high resolution confocal microscopy. In the study reported by McNally *et al*²⁵, the sensitivity to imaging is questionable by the use of exogenous fluorescent dyes, and time may be an issue when collecting *in vivo* images throughout the distal colon. The three modalities (OCT, LIF, LSCM) were used in combination for the elucidation of the analytical results, yet OCT, which is an imaging technique capable of cellular resolution, could not discern the colonic crypts in their experimentation. The difference between their scheme and our imaging paradigm (OCT + FMI) is that we are able to resolve anatomy, including crypts at 10 μ m detail.

In our studies, the TEM (Figure 5) shows both spherical and tubular surface morphology of the liposomes. Our initial expectations were to observe spherical liposomes. Experimental examination led to the finding that the mixture of the two types of lipids during synthesis (DAPC and DMPC or DMPE-GLU) yields a mixed-batch liposomal morphology. According to Yager *et al*²⁶ a polymerizable diacetylenic monomeric (e.g. DAPC) lipid will form a hollow tube when cooled slowly through its phase transition temperature (T_m). Additionally, Markowitz *et al*²⁷ portray a scheme of mixed polymers (DC_{8,9}PC and DNPC), with a braid-like morphology at different salt and DNPC concentrations; as the molar percentage of DNPC enlarged, the morphology of the structures became increasingly spherical. It therefore, appears that the mixed liposomal morphology is reasonable.

Rh-I-UEA-1 binds polyps without washing away, in contrast to the phenomenon occurring at the normal adjacent mucosa, where Rh-I-UEA-1 binds and washes away. Adenomatous polyps may generate more surface mucin than normal mucosa, thereby providing more binding prospects between α -L-fucose and UEA-1. In addition, we have found, using OCT + FMI, a ring-like labeling around the perimeter of the polyps with Rh-I-UEA-1. This phenomenon was observed in > 50 % of specimens. To our knowledge, this ring-like labeling has not been described elsewhere in the literature. This evidence further substantiates Rh-I-UEA-1 as a surface tag for polyp detection.

Rh-I-UEA-1 also has implications as an optical marker for colonoscopy. Here, we describe incorporation of the fluorescent probe Rhodamine B within polymerized liposomes, and its successful discrimination between adenomatous and normal adjacent tissue using MSI and OCT. Other groups have demonstrated colonoscopy using fluorescein-labeled markers and endoscopy. For example, Hsiung *et al*²⁸ screened phage display peptides against fresh human colonic adenomas to identify a sequence with preferential binding to premalignant tissue. A specific fluorescein-conjugated peptide sequence was imaged *in vivo* using a fluorescence confocal microendoscope (through a standard colonoscope) in patients undergoing colonoscopy. The authors²⁸ found the fluorescein-conjugated peptide bound

dysplastic colonocytes with 81 % sensitivity, 82 % specificity versus normal adjacent mucosa. In another study, Funovics *et al*²⁹ reported *in vivo* mouse colonoscopy using a 2-channel real-time fluorescence microendoscopy imaging system. A protease activated NIR fluorescent probe and a NIR nonactivated perfusion probe were used to correlate healthy colon, adenoma or adenocarcinoma tissue with the concentration of cathepsin B (overexpression correlates with metastasis and angiogenesis in human CRC³⁰⁻³¹); paradigms used to study the lesions were the APC^{Min+/-} model of adenoma and a model of adenocarcinoma created by orthotopically implanting murine colon cancer CT26 cells against a nude background. The authors confirmed an increased imaging ratio of protease activity/perfusion across the spectrum from healthy colon to adenoma to adenocarcinoma²⁹.

Our CT imaging experiments could have been improved with either an imaging agent with an increased saturation point (Omnipaque = 350mg/mL I), or a vesicle that would allow a greater iodine carrying capacity, for improved discrimination between polyp and normal tissue. Although the iodine imaging source, Omnipaque, distinguished normal and polyp tissue based on the UEA-1 target, we found the liposome loading capacity of iodine too low to provide sufficient discrimination.

5. Summary

Novel polyp specific Rh-I-UEA-1 liposomes were polymerized to target and image adenomatous polyps in the APC^{Min/+} mouse. Rh-I-UEA-1 had a significantly greater labeling efficiency versus control liposomes, which was verified by MSI and OCT+FMI. These results may have clinical significance for the improvement of sensitivity of polyp detection on CTC in CRC diagnosis.

Acknowledgments

This research was supported by the Intramural Research Programs of the NIH Clinical Center (CC), National Heart Lung and Blood Institute (NHLBI), and the National Institute of Diabetes and Digestive and Kidney Diseases (NIDDK). We thank Dr. Matt Dreher and Dr. Lawrence Tabak for helpful discussions, Dr. Mari Kono and Dr. Richard Proia for providing mice, and Dr. Shijun Wang for help in preparing statistical analyses.

References

1. O'Brien MJ, O'Keane JC, Zauber A, Gottlieb LS, Winawer SJ. Precursors of colorectal carcinoma. Biopsy and biologic markers. *Cancer*. 1992; 70:1317–1327. [PubMed: 1511379]
2. Yonezawa S, Nakamura T, Tanaka S, Sato E. Glycoconjugate with Ulex europaeus agglutinin-I-binding sites in normal mucosa, adenoma, and carcinoma of the human large bowel. *J Natl Cancer Inst*. 1982; 69:777–785. [PubMed: 6181281]
3. Caldero J, Campo E, Vinas J, Cardesa A. Lectin-binding sites in neoplastic and non-neoplastic colonic mucosa of 1,2-dimethylhydrazine-treated rats. *Lab Invest*. 1989; 61:670–676. [PubMed: 2689774]
4. Chen H, Torchilin V, Langer R. Lectin-bearing polymerized liposomes as potential oral vaccine carriers. *Pharm. Res*. 1996; 13:1378–1383. [PubMed: 8893278]
5. Fabani MM, Gargini R, Taira MC, Lacono R, Alonso-Romanowski S. Study of in vitro stability of liposomes and in vivo antibody response to antigen associated with liposomes containing GM1 after oral and subcutaneous immunization. *J Liposome Res*. 2002; 12:13–17. [PubMed: 12604034]
6. Alonso-Romanowski S, et al. Characterization of diacetylenic liposomes as carriers for oral vaccines. *Chem Phys Lipids*. 2003; 122:191–203. [PubMed: 12598052]
7. Andrews PM, et al. High-resolution optical coherence tomography imaging of the living kidney. *Lab Invest*. 2008; 88:441–449. [PubMed: 18268476]
8. Yuan S, et al. Combining optical coherence tomography with fluorescence molecular imaging: towards simultaneous morphology and molecular imaging. *Proceedings of the SPIE*. 2009; 7169: 716900-716900/1-6. [PubMed: 191698]

9. Rhodes DG, Singh A. Structure of polymerizable lipid bilayers IV: mixtures of long chain diacytlenic and short chain saturated phosphatidylcholines and analogous asymmetric isomers. *Chem. Phys. Lipids*. 1991; 59:215–224. [PubMed: 1804565]
10. O'Connor SD, Summers RM, Choi JR, Pickhardt PJ. Oral contrast adherence to polyps on CT colonography. *J Comput Assist Tomogr*. 2006; 30:51–57. [PubMed: 16365572]
11. Pickhardt PJ, Choi JH. Electronic cleansing and stool tagging in CT colonography: advantages and pitfalls with primary three-dimensional evaluation. *AJR Am J Roentgenol*. 2003; 181:799–805. [PubMed: 12933484]
12. Nicoloff DM, Ellis CM, Humphrey EW. Management of villous adenomas of the colon and rectum. *Arch Surg*. 1968; 97:254–260. [PubMed: 5657430]
13. Hoskins LC. Human enteric population ecology and degradation of gut mucins. *Dig Dis Sci*. 1981; 26:769–772. [PubMed: 7285743]
14. Gold DV, Miller F. Characterization of human colonic mucoprotein antigen. *Immunochemistry*. 1974; 11:369–375. [PubMed: 4477551]
15. Forstner JF, Forstner GG. Calcium binding to intestinal goblet cell mucin. *Biochim Biophys Acta*. 1975; 386:283–292. [PubMed: 236024]
16. Kocer B, et al. Expression of MUC5AC in colorectal carcinoma and relationship with prognosis. *Pathol Int*. 2002; 52:470–477. [PubMed: 12167106]
17. Wesseling J, van der Valk SW, Hilkens J. A mechanism for inhibition of E-cadherin-mediated cell-cell adhesion by the membrane-associated mucin episialin/MUC1. *Mol Biol Cell*. 1996; 7:565–577. [PubMed: 8730100]
18. Ajioka Y, Watanabe H, Jass JR. MUC1 and MUC2 mucins in flat and polypoid colorectal adenomas. *J Clin Pathol*. 1997; 50:417–421. [PubMed: 9215126]
19. Nakamori S, Ota DM, Cleary KR, Shirohani K, Irimura T. MUC1 mucin expression as a marker of progression and metastasis of human colorectal carcinoma. *Gastroenterology*. 1994; 106:353–361. [PubMed: 7905449]
20. Boland CR, Montgomery CK, Kim YS. Alterations in human colonic mucin occurring with cellular differentiation and malignant transformation. *Proc Natl Acad Sci U S A*. 1982; 79:2051–2055. [PubMed: 6952252]
21. Rogart JN, et al. Multiphoton imaging can be used for microscopic examination of intact human gastrointestinal mucosa ex vivo. *Clin Gastroenterol Hepatol*. 2008; 6:95–101. [PubMed: 18065276]
22. Muguruma N, Ito S. Labeled anti-mucin antibody detectable by infrared-fluorescence endoscopy. *Cancer Biomark*. 2008; 4:321–328. [PubMed: 19126960]
23. Sodik NM, et al. Smad3 deficiency promotes tumorigenesis in the distal colon of ApcMin/+ mice. *Cancer Res*. 2006; 66:8430–8438. [PubMed: 16951153]
24. Hariri LP, et al. Endoscopic optical coherence tomography and laser-induced fluorescence spectroscopy in a murine colon cancer model. *Lasers Surg Med*. 2006; 38:305–313. [PubMed: 16596657]
25. McNally JB, et al. Task-based imaging of colon cancer in the Apc(Min/+) mouse model. *Appl Opt*. 2006; 45:3049–3062. [PubMed: 16639453]
26. Yager P, Schoen P, Davies C, Price R, Singh A. Structure of lipid tubules formed from a polymerizable lecithin. *Biophysical journal*. 1985; 48:899–906. [PubMed: 19431600]
27. Markowitz MA, Singh A, Chang EL. Formation and properties of a network gel formed from mixtures of diacytlenic and short-chain phosphocholine lipids. *Biochem Biophys Res Commun*. 1994; 203:296–305. [PubMed: 8074670]
28. Hsiung PL, et al. Detection of colonic dysplasia in vivo using a targeted heptapeptide and confocal microendoscopy. *Nat Med*. 2008; 14:454–458. [PubMed: 18345013]
29. Funovics MA, Alencar H, Montet X, Weissleder R, Mahmood U. Simultaneous fluorescence imaging of protease expression and vascularity during murine colonoscopy for colonic lesion characterization. *Gastrointest Endosc*. 2006; 64:589–597. [PubMed: 16996355]
30. Kruszewski WJ, et al. Overexpression of cathepsin B correlates with angiogenesis in colon adenocarcinoma. *Neoplasma*. 2004; 51:38–43. [PubMed: 15004658]

31. McKerrow JH, et al. A functional proteomics screen of proteases in colorectal carcinoma. *Mol Med.* 2000; 6:450–460. [PubMed: 10952024]

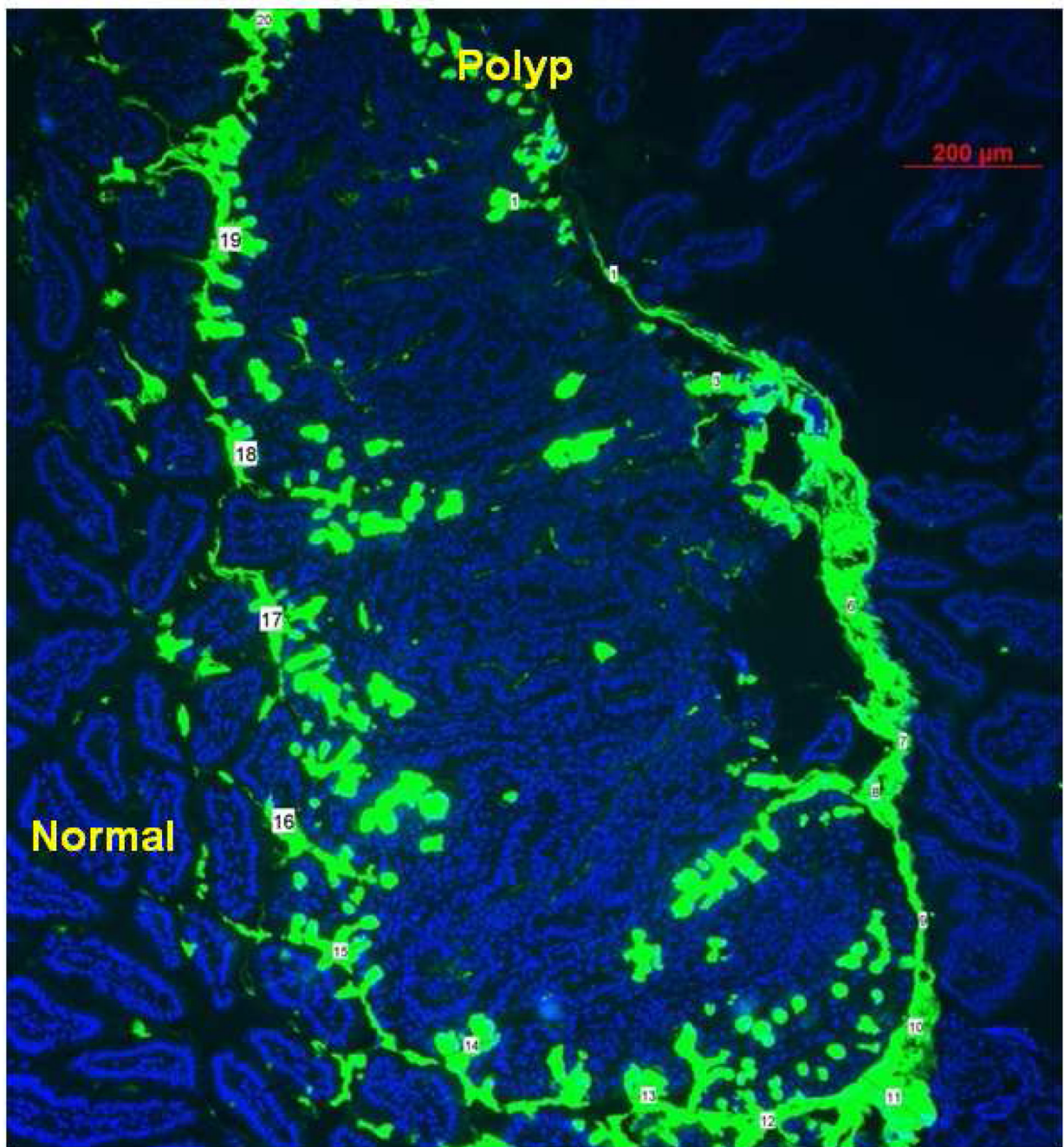


Figure 1. FITC-UEA-1 lectin shows excellent differential glycoprotein expression between polyp and normal cells. Numbers mark where mucin layer was measured (ImageJ processing software). Average measurement of mucin layer was $53.44 \pm 27.03 \mu\text{m}$.

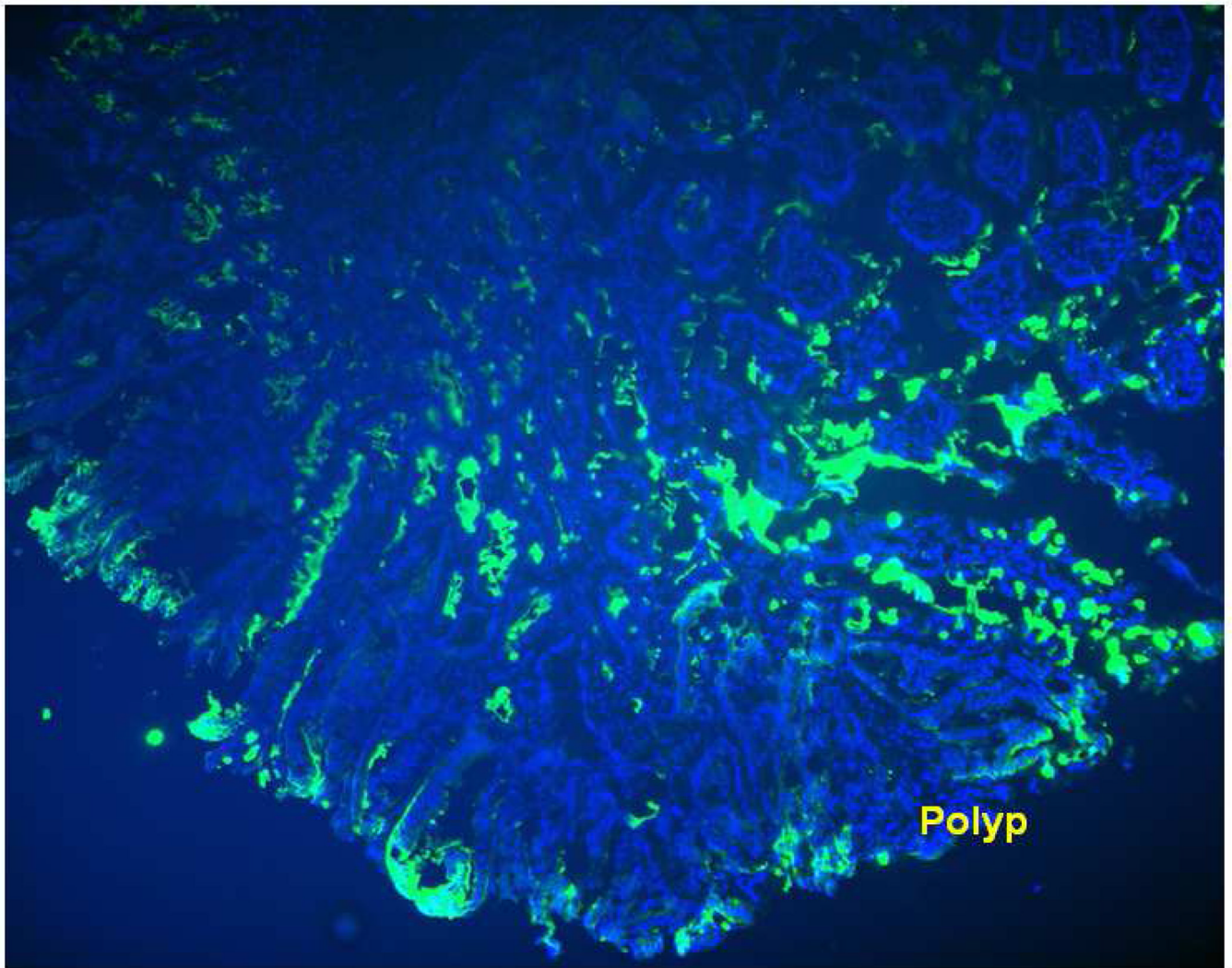


Figure 2. FITC-UEA-1 binds to the surface of the polyp even when the colon is incubated prior to slicing, thus confirming that the lectin is a viable ligand for surface targeting of the polyps in APC Min^{+/+} specimen.

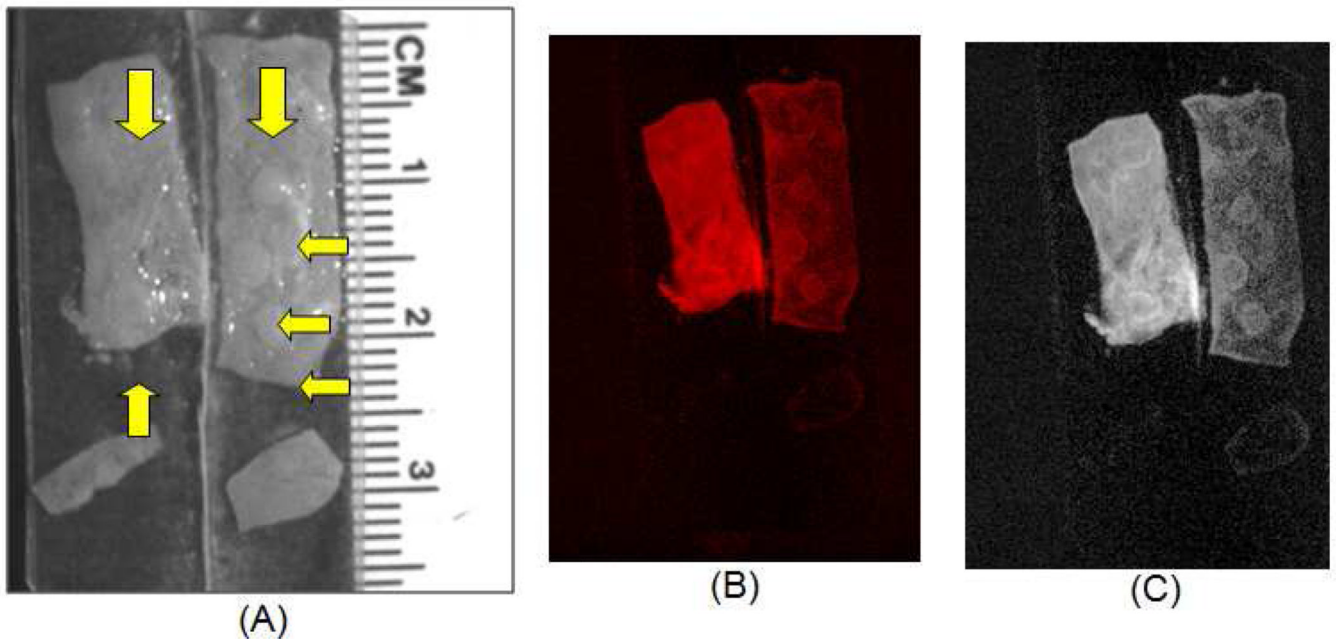


Figure 3. Ex vivo multispectral optical imaging of excised APC Min^{+/} tissue incubated in Rh-IUEA-1 targeted liposomes (A: right) or control liposomes (no UEA-1; A: left); yellow arrows indicate polyps. Rh-I-UEA-1 targeted liposomes show specificity towards polyps in APC Min^{+/} tissue, as seen with incorporated rhodamine contrast agent (B), and with background subtraction (C).

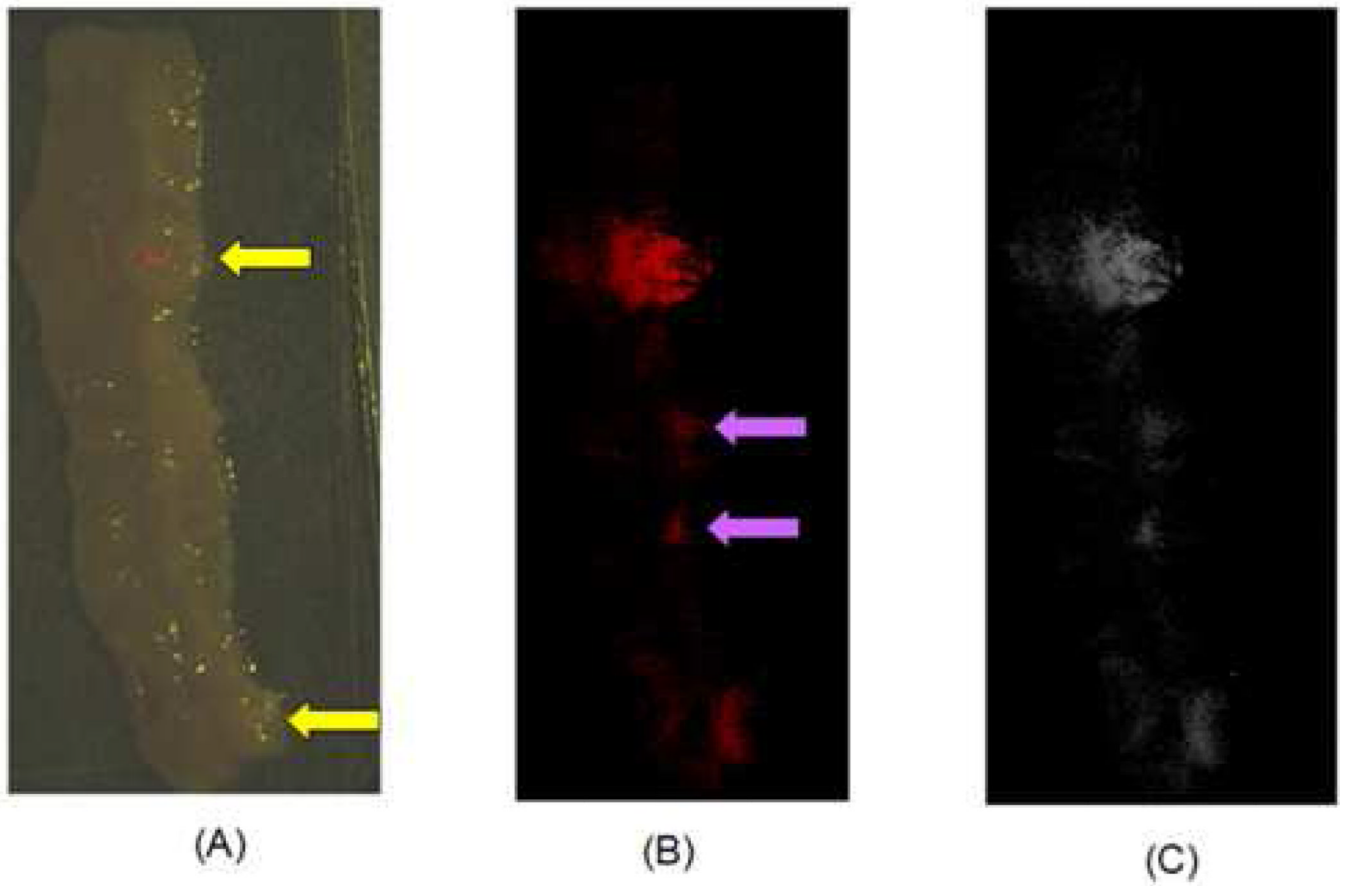
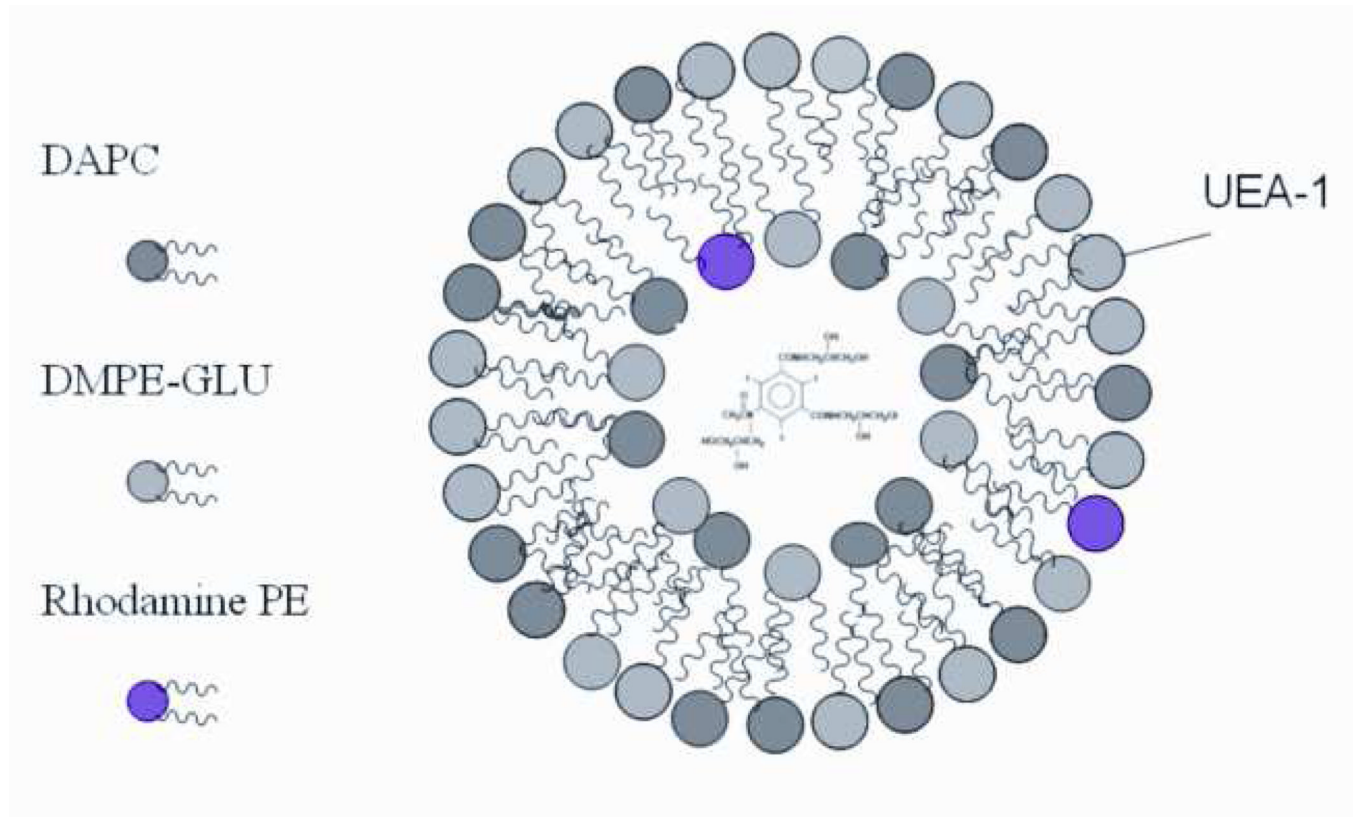


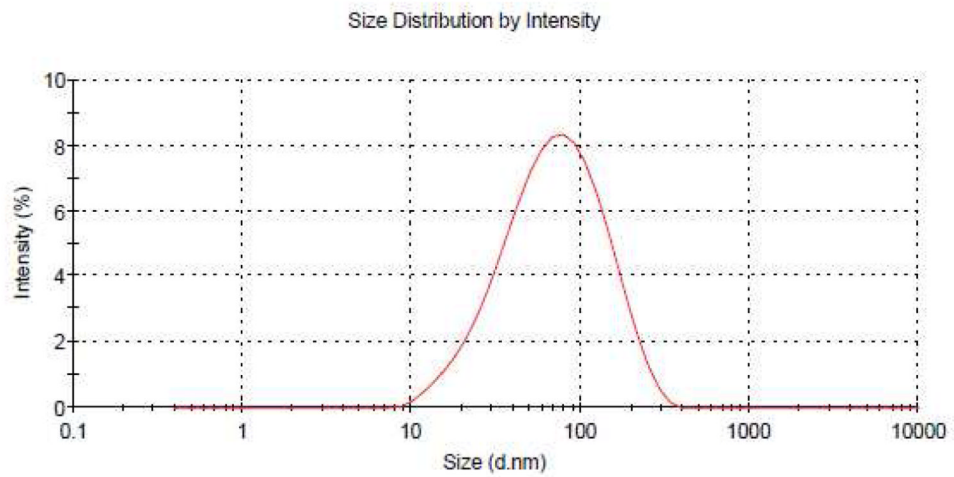
Figure 4. Optical image of liposomal binding. Rh-I-UEA-1 liposomes have greater specificity towards polyps (shown as yellow arrows in bright field image A) versus nonspecific binding of normal mucosa (shown as purple arrows in fluorescent image B) in APC Min^{+/−} tissue; image C shows background subtraction.



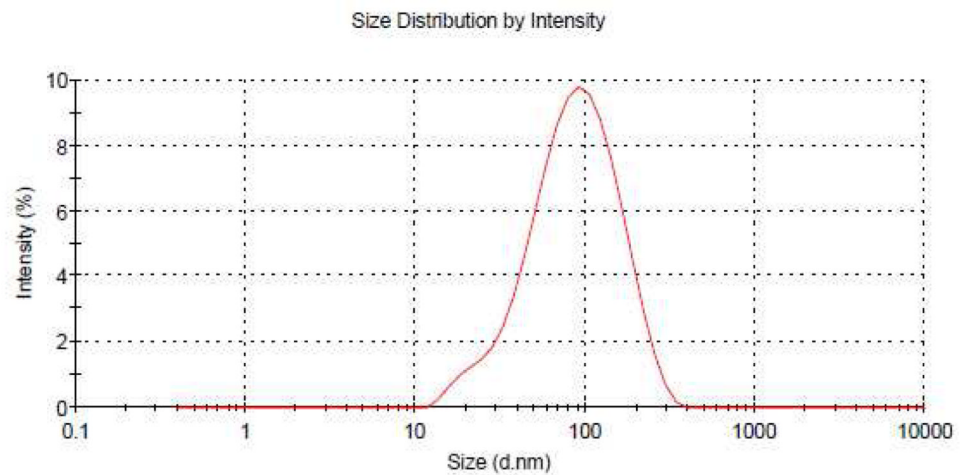
5. (A) Pictorial representation of the liposomes.

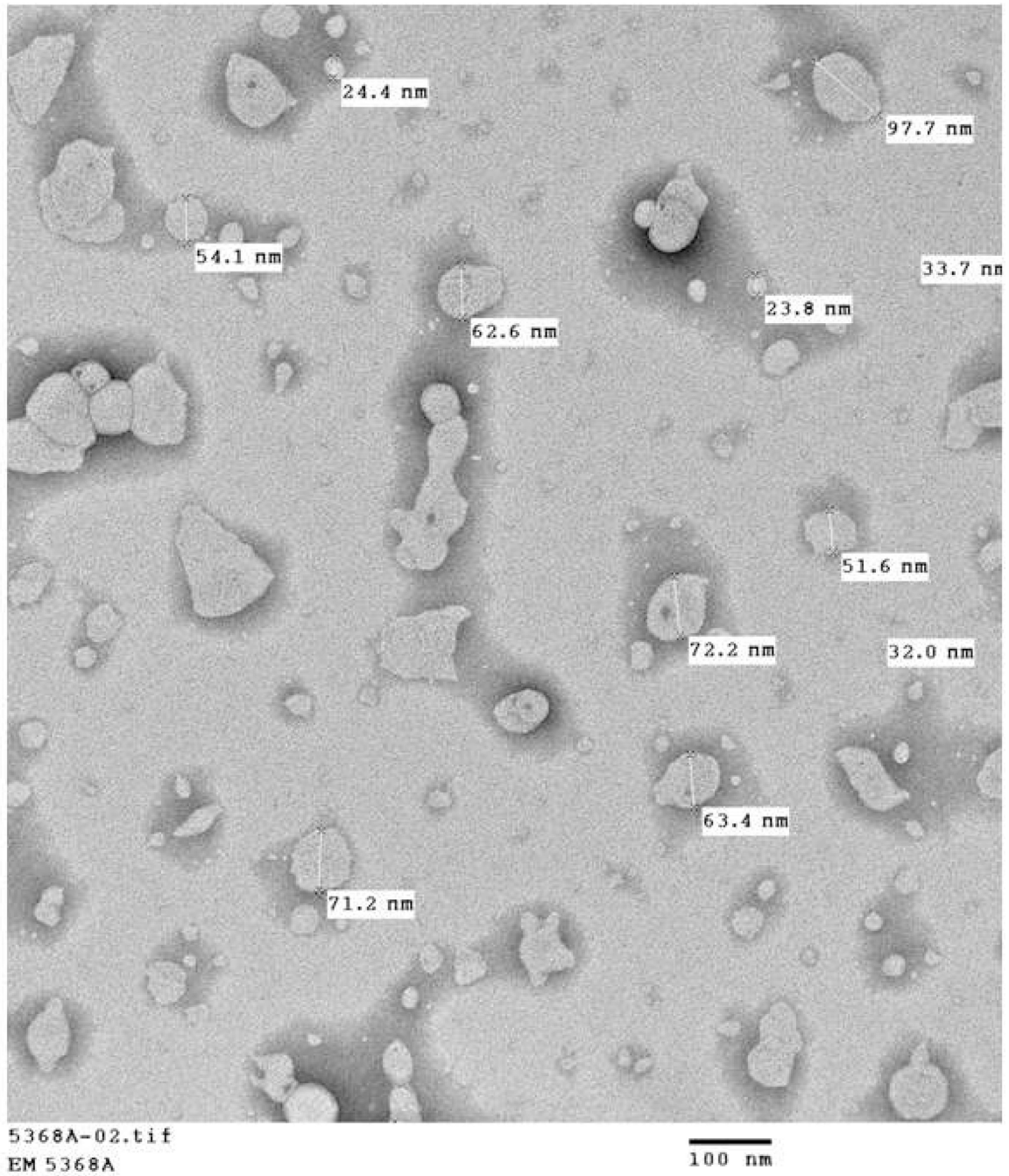
5b. DLS analysis of Control and UEA-1 conjugated liposomes

Control Liposomes

Z-Average (d.nm): 57.30**Pdl: 0.276**

UEA-1 Liposomes

Z-Average (d.nm): 73.21**Pdl: 0.263**



5d. HPLC analysis of UEA-1 Liposomes

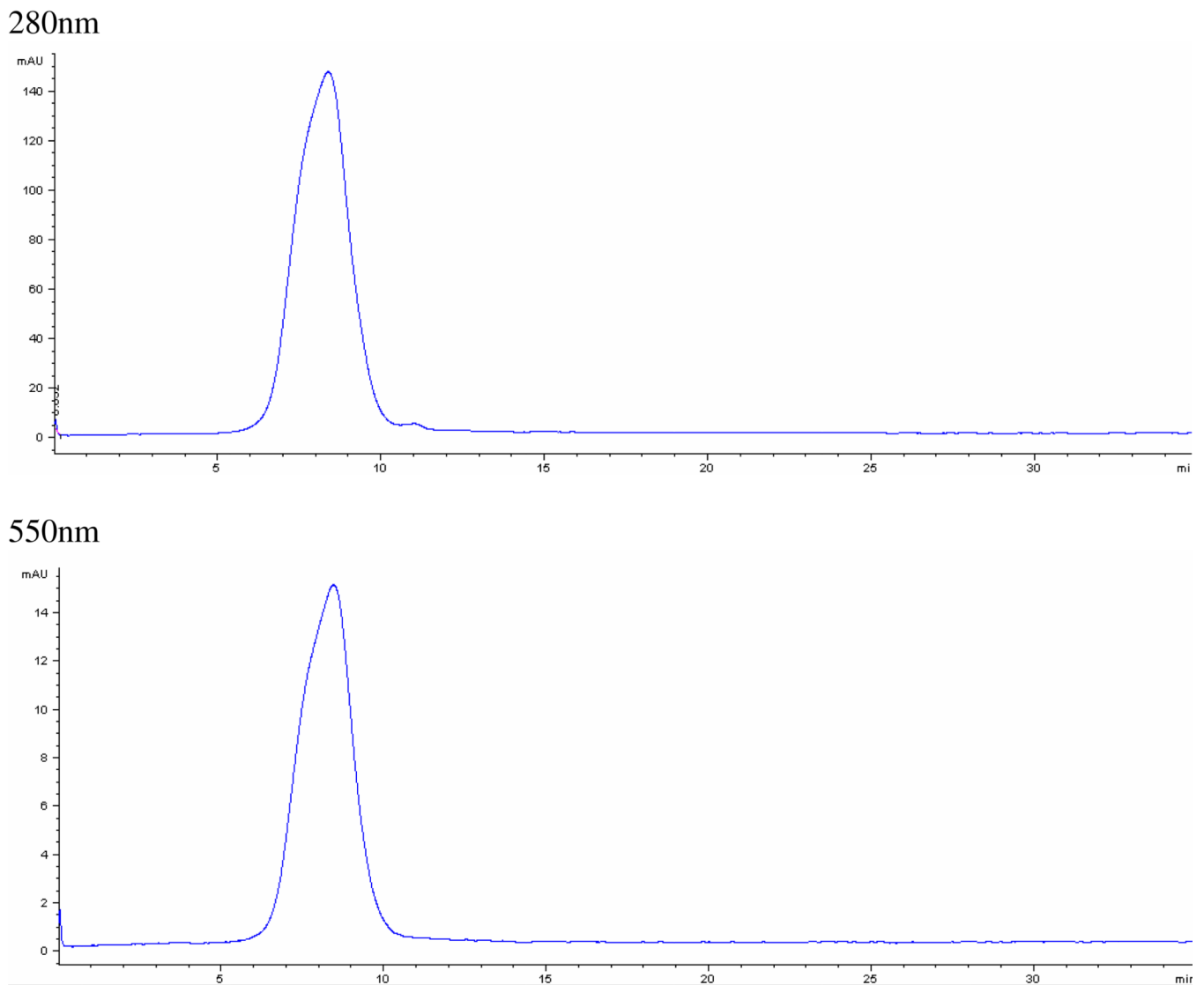


Figure 5. (A) Pictorial representation of the liposomes. (B) Representative DLS of control and UEA-1 conjugated liposomes. (C) Transmission electron micrograph (TEM) of liposomes showing spherical and tubular morphology due to mixing of two types of lipids; average size is 53.34 ± 23.20 nm. (D) HPLC of purified UEA-1 liposomes (retention time 8.4min).

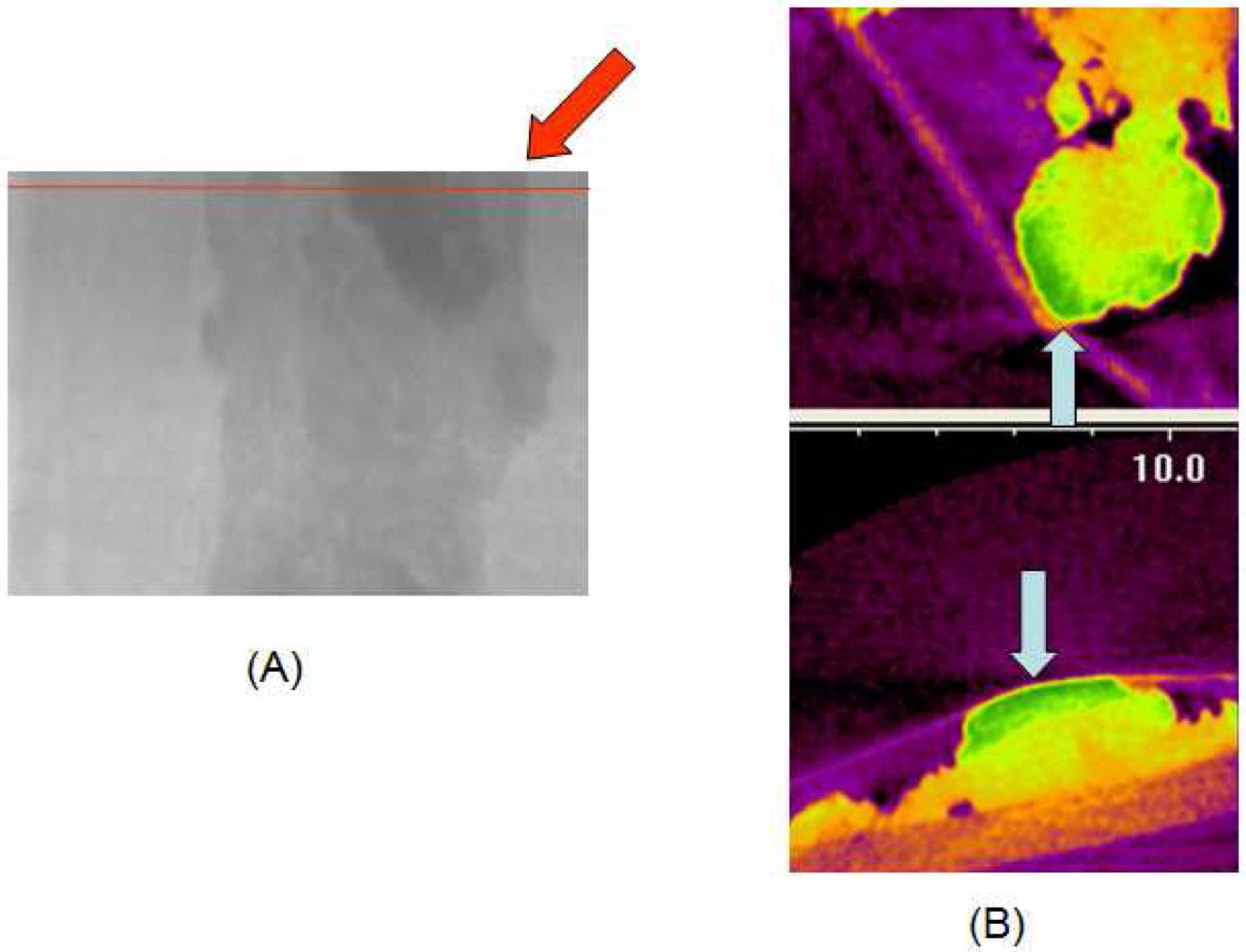
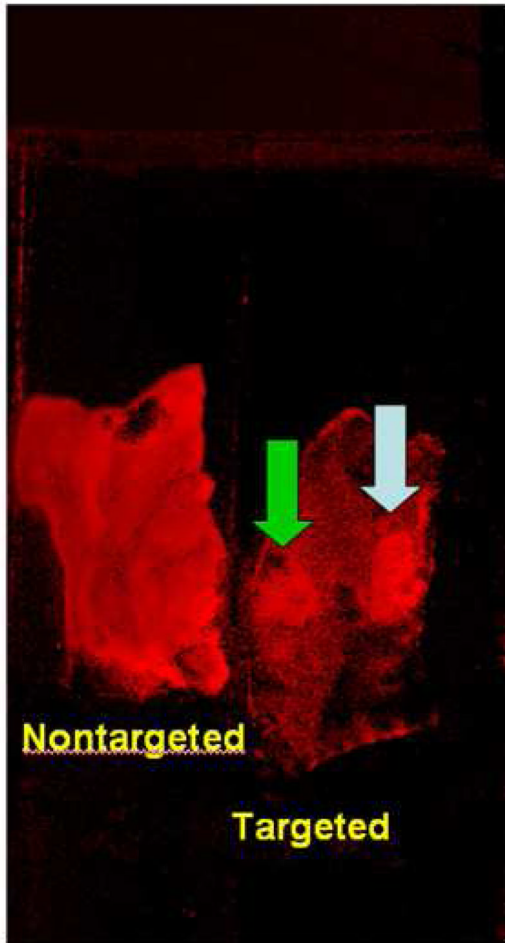


Figure 6. CT image of a polyp (A, red arrow) incubated with Rh-I-UEA-1. Blue arrows show the surface of the polyp. Transaxial slices were taken (A, red line); 3D images are shown. Y (B, top) and Z (B, bottom) orientations are shown. In (B), images are false color cross-sections taken from the imaging volume.

Multispectral Optical Imaging (MSI)



Optical Coherence Tomography (OCT) with Fluorescence Molecular Imaging (FMI)

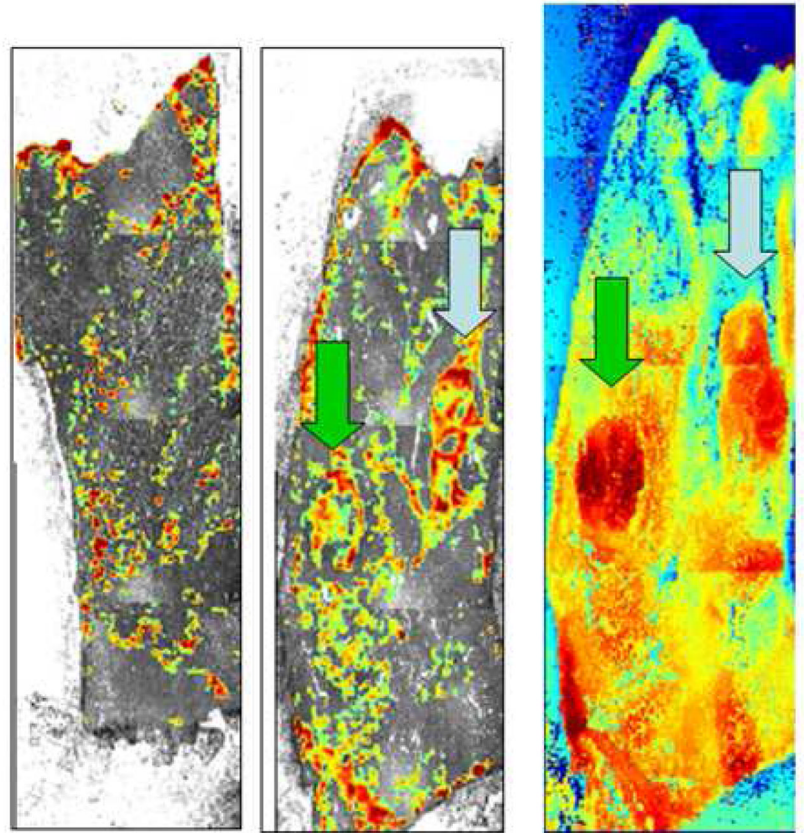


Figure 7.

Rh-I-UEA-1 targeted liposomes bind APC $Min^{+/}$ adenomatous polyps. Binding is greater in polyps (arrows) versus normal mucosa (MSI, left); binding by nontargeted liposomes (OCT + FMI, right) is less than by targeted liposomes (Middle). Third OCT panel (C) is a height profile of tissue in targeted in image, and is used in polyp localization.

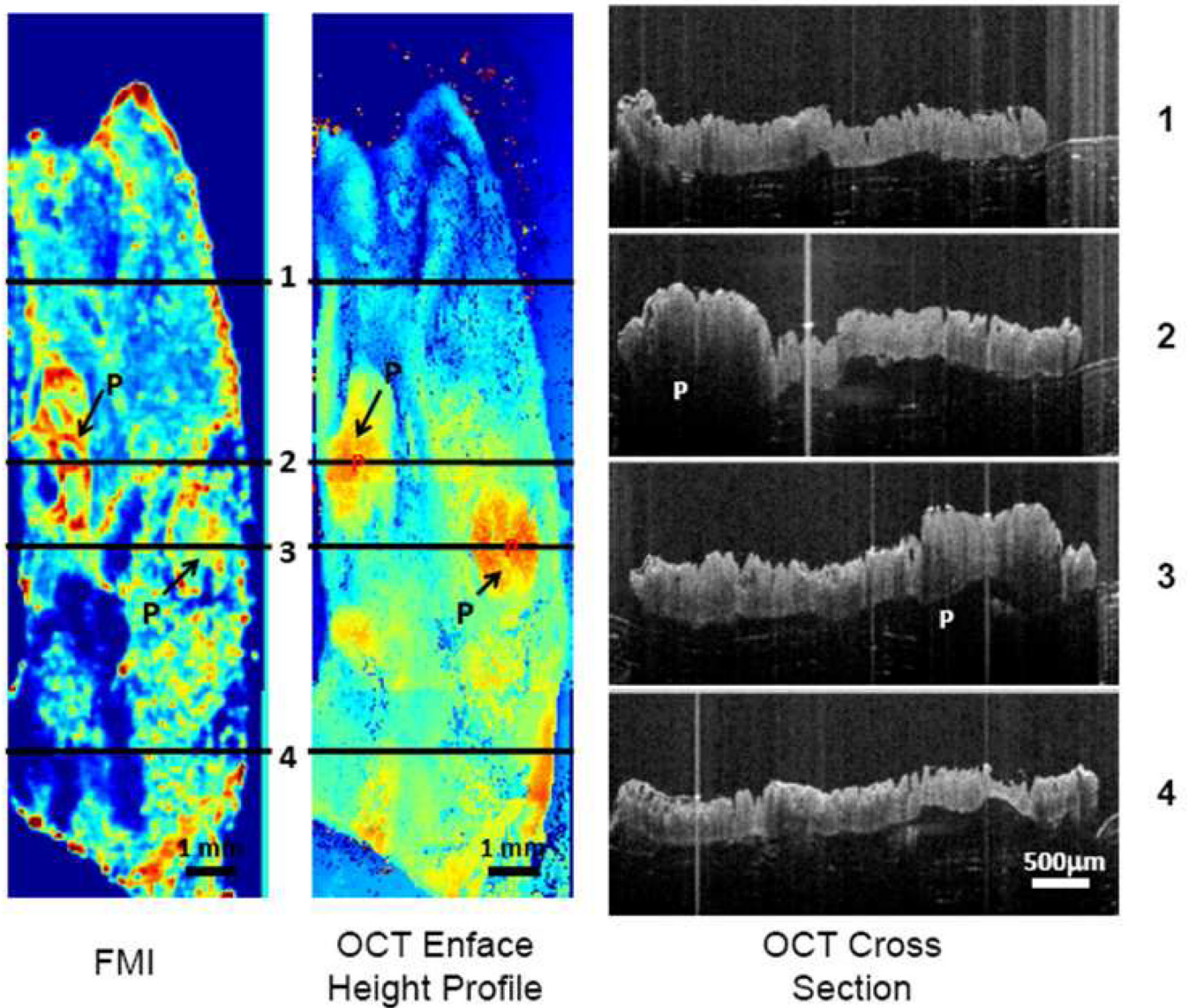


Figure 8. Fluorescence image (FMI) and OCT Enface height profile image from conjugated sample. Also shown in the image are four OCT cross section images from lines 1, 2, 3 and 4 in the OCT enface height image. "P" in the images indicates polyp regions.

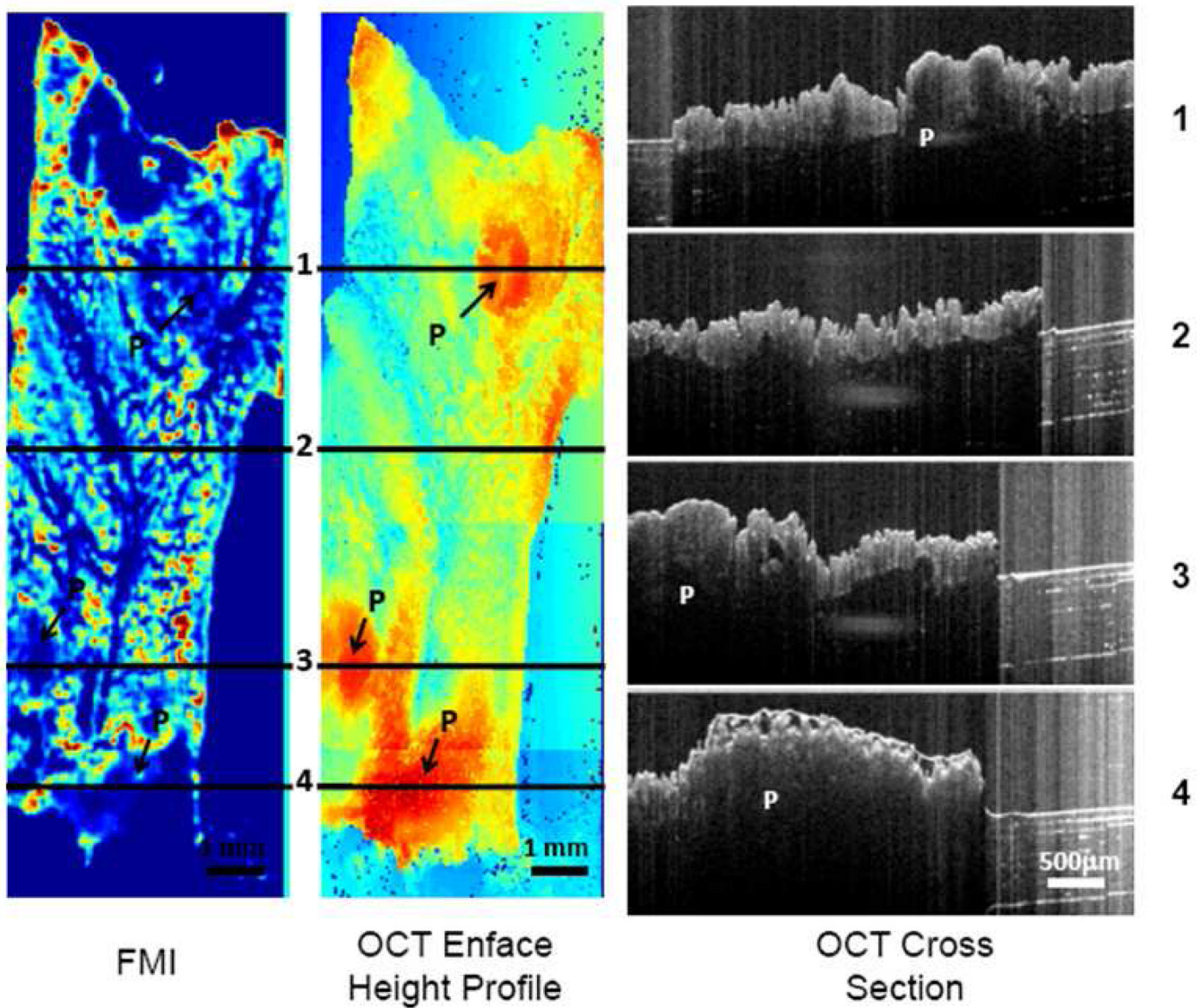


Figure 9.

Fluorescence image (FMI) and OCT enface height profile image from nonconjugated sample. Also shown in the figure are four OCT cross section images from lines 1, 2, 3 and 4 in the OCT enface height image. "P" in the images indicates polyp regions.